DARK MATTER TOMOGRAPHY

Tony Tyson
Bell Labs, Lucent Technologies
Murray Hill, NJ 07974

ABSTRACT

Over cosmic time the small fluctuations in dark matter density in the early Universe grew via gravitational instability. Until recently our view of this process has been indirect, relying on radiation from the small baryonic component. If we could measure directly the development of these mass overdensities over a range of scales and look-back times, cosmology and the nature of the dark matter would be constrained in a new way.

Gravitational lensing provides an opportunity to image directly these dark matter concentrations. This article is a short tutorial and review of recent progress in strong and weak gravitational lens tomographic imaging of dark matter. The lens-distorted images of background galaxies are inverted, yielding a two-dimensional map of the projected dark matter overdensity. The maps cover a range of scales and thus constrain the nature of dark matter. On 10 kpc scales, high resolution strong lens inversions reveal a soft core in the mass distribution, unexpected in scale-free cold dark matter N-body simulations. On 10 Mpc scales, statistical weak lensing inversion maps of mass show the outer mass profile of overdensities in the linear regime. These weak lensing studies, using mosaics of CCDs, are opening a new window on the Universe.

1 Cosmological Motivation

Cosmology is in the midst of a revolution. As exciting new observational techniques and experiments loom on the horizon, the current observations have already replaced the standard cosmology of the 1980s with a new cosmology. In turn, this new cosmology raises very different questions about the nature of mass and energy in the Universe. Defining Ω as the sum over all forms of mass-energy, we can summarize the paradigm shift by listing the key parameters. Indeed, the parameter list itself is changing as old parameters are pinned down and new ones are forced on us.

Standard Cosmology (1980s):

$$\Omega = 1$$

$$H_0 = 50 - 100$$

$$\Lambda = 0$$

$$\Omega_{matter} \approx \Omega_{WIMP,axion} \sim 1 >> \Omega_{baryon}$$

Current Model (1998):

$$\Omega_{matter} \approx \Omega_{WIMP,axion} \approx 0.2 - 0.4 >> \Omega_{baryon}$$

$$H_0 = 67 \pm 10$$

Either $\Omega \neq 1$ or $\Lambda \neq 0$

Either way, we are led to new physics. The nature and distribution of dark matter plays a central role. Ω_m has been obtained mainly through extrapolating indirect observations of luminous clusters of galaxies to the rest of the Universe. If we could pin down Ω_m via a direct observation, this would significantly clarify cosmology. It may be premature to conclude that we have accounted for most all the dark matter, since until very recently we have relied on the notion that radiation traces mass.

Inflation theories are based on a flat Universe as suggested by the high degree of isotropy of the cosmic microwave background: total energy density equal to the critical density. Since ordinary matter (baryons) contributes only about 5% of the critical density, there must be something else. The leading candidate is relic, elementary particles. Generically, they fall into two classes: relativistic "hot" dark matter, and non-relativistic "cold" dark matter. Neutrinos of rest mass 30 eV or so are the prime examples of hot dark matter; they move quickly because they were once in thermal equilibrium and are very light. Axions and neutralinos are examples of cold dark matter. Neutralinos move slowly because they too were once in thermal equilibrium and they are very heavy. Axions are extremely light, but were never in thermal equilibrium (having been produced very cold).

Some candidates for the non-baryonic dark matter fit the observed large scale structure less well than others. Relativistic hot dark matter, such as neutrinos with a small rest mass (30 eV would be cosmologically significant), form structure from the top down and too late. Neutrinos also free stream [Landau damping or collisionless phase mixing] on galaxy scales, suppressing galaxy formation via gravitational instability. Observations very clearly indicate that galaxies formed at redshifts $z \sim 2 - 5$, before superclusters which are just forming today. So hot dark matter is not a major component of the dark matter.[1]

Nonrelativistic weakly interacting elementary particles (so-called Cold Dark Matter) work better. Cold Dark Matter (CDM) allows structure to form earlier via bottom-up hierarchical accretion onto dark matter overdensities. Given enough time (old enough Universe) and the right initial spectrum of density fluctuations, it ought to be possible to account for the observed structure evolution. Cold dark matter particles cannot move far enough to damp perturbations on small scales, and structure then forms from the bottom up: galaxies, followed by clusters of galaxies, and so on.[2] For a mass fluctuation spectrum normalized to the cosmic microwave background anisotropies found by the COBE satellite, most galaxies should have formed around redshifts $z \sim 2-4$, just as recent observations indicate. For example, evidence for early structure formation is shown in Fig. 1 where the star formation rate gleaned from studies of distant galaxies and quasars is shown vs look-back time or redshift.

At present, the cold dark matter + inflation scenario looks promising since it is consistent with a large body of observations: measurements of the anisotropy of the cosmic background radiation (CBR), redshift surveys of the distribution of matter today, and deep probes of the Universe. However, observations have hardly begun to discriminate between different inflationary models and versions of CDM. At the moment, we can say that the data favor a flat Universe, almost scale-invariant density perturbations, and cold dark matter with a small admixture of baryons.

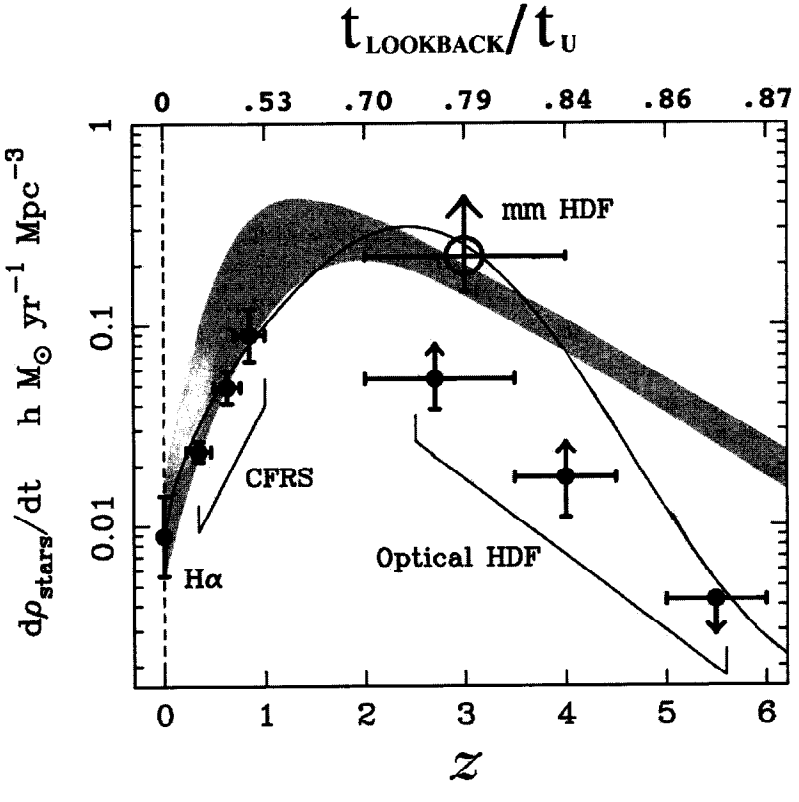

Fig. 1. Star formation vs look-back time or redshift, from studies of galaxies and quasars. The optical Hubble Deep Field data have not been corrected for dust absorption in this plot. These distant objects, if resolved, may be used as tools for measuring intervening mass concentrations.

Surprisingly, simulations of structure formation based on "standard" $\Omega = 1$ CDM with scale-free Gaussian initial fluctuations and zero cosmological constant still make galaxy clusters too late. When normalized to the CMB fluctuations on the 10^3 Mpc scale found by COBE, standard CDM produces too much power today on scales of galaxy clusters, creating relatively too few rich clusters at redshift 0.5. Indeed, a successful detailed model of structure formation must be compatible with the existence of galaxies at redshifts greater than 5, as well as the observed number densities of clusters of galaxies vs redshift.

Most of the matter in the Universe is of unknown form and dark: Stars (and related material) contribute a tiny fraction of the critical density, $\Omega_{\rm lum} = 0.003 \pm 0.001h^{-1} \sim 0.004$, while the amount of matter known to be present from its gravitational effects contributes around 100 times this amount, $\Omega_{matter} = 0.3 \pm 0.1$. The gravitational mass of dark matter is needed to hold together everything large in the Universe: galaxies, clusters of galaxies, and superclusters. A variety of methods for determining the amount of matter all seem to converge on $\Omega_{matter} \sim 1/3$; they include measurements of the masses of clusters of galaxies and the peculiar motions of galaxies. It is the prospect of directly measuring Ω_m and mass structure that is the subject of these notes.

Finally, the theory of Big Bang nucleosynthesis and the recently measured primeval abundance of deuterium[3] tightly constrain the baryon density: $\Omega_{baryon} = (0.02 \pm 0.002)h^{-2} \sim 0.05$. The factor of ten discrepancy between this number and dynamical and lensing measurements of the matter density is evidence for nonbaryonic dark matter.

2 Historical Perspective

Dark matter leads to large scale structure formation, via gravitational instability. Today, our task is to find out how much there is and where it is. Historically, the realization (not widely shared at the time) that large structures, clusters of galaxies, were dominated by non-luminous matter came in the 1930s. Fritz Zwicky, shown in Figure 2, found an amazingly high dispersion in radial velocities of galaxies in a cluster; about an order of magnitude larger than expected from the virial theorem if each solar luminosity was assigned one solar mass.[4,5] Zwicky went on to suggest a number of gravitational lens investigations using galaxies as lenses, which are just being done now. It took 30 years for the next decisive step

Fig. 2. Fritz Zwicky, late 1960s. Courtesy Wal Sargent.

and for the real beginning of acceptance by the scientific community of the notion that most of the mass in the Universe is dark.

In the 1960s Vera Rubin and Kent Ford were taking spectra of nearly edge-on spiral galaxies, using the new image intensifiers and a long slit placed along the plane of each galaxy. The resulting radial velocity as a function of position through the galaxy looked pathological; they found non-Keplerian orbits for stars and gas in spiral galaxies, implying an enclosed mass rising $\sim r$, and dark massive halos. While the nuclei of these galaxies were optically luminous, the mass seemed to be mostly in a diffuse outer halo where there was little or no light. As the debate over the amount of mass in the Universe and distribution of mass within galaxies raged, some began to ponder the observational consequences of a "plum pudding" Universe[6] and heavy galaxies. In 1973, Press and Gunn showed[7] that $\Omega \sim 1$ in dark compact objects would produce too many "Einstein rings." Today the outer extent of galaxy dark matter halos is still an open question, although the volume normalized galaxy mass in a large volume is understood to be much less than the critical mass density.

The first cosmic mirage was discovered by Walsh *et al.* in 1979:[8] they found a doubly lensed quasar Q0957+561. The lens, a foreground galaxy with a massive dark halo, produces two bright images of the same quasar (presumably in addition to a third, highly demagnified image)—an example of strong gravitational lensing. This event, happening as it did in the midst of speculation about dark matter halos, ushered in the era of gravitational lensing. In the following decade, lensing evolved from a curious rare phenomenon into an astrophysical tool. On the theoretical front, it was realized in the 1980s that dominant mass dark halos were good: they stabilize galaxy stellar disks. Technology drove new observations. Like the introduction of the image intensifier in the 1960s, the debut of the CCD in astronomy would have consequences for our understanding of dark matter. Our discovery of the faint blue galaxies (first a hint with deep photographic plates, and then their obvious presence in CCD images in the early 1980s) immediately suggested their use as a tool in studying dark matter via statistical weak gravitational lensing.

Another form of strong gravitational lensing, but this time with resolved background galaxies, was discovered in clusters of galaxies in 1987 nearly simultaneously by two groups (Lynds and Petrosian in the US, and Soucail *et al.*in France). A single background galaxy is heavily distorted into one or more long arcs con-

centric with the mass centroid of the cluster. This type of strong lensing forms the basis of the highest resolution mass maps (see below).

Today, we have two kinds of dark matter, and two problems. Hot and cold. Baryonic and non-baryonic. Most of the baryonic matter is dark, and most of the dark matter is non-baryonic. A key problem with viewing our Universe with traditional techniques (velocity dispersion, X-ray gas luminosity) is that we have been literally looking under lamp posts. So it is necessary to take what we currently know about the mass content of the Universe with a degree of caution. With the new tool of gravitational lens tomography, there are several questions that may be addressed: Have we found it all? Perhaps there is dark matter outside luminous clusters and superclusters. We already know mass-light segregation occurs on some scales. Does the distribution of mass inside clusters agree with the N-body theory predictions? Cold dark matter is scale-free. Does the mass halo cut off sharply at large radius? What about the vast volume in between clusters? Is there dark matter there and what are its morphological properties? Fundamentally, we need to weigh space. Given that no complete survey of mass by lensing has yet been done, we must remain open minded. Is $\Omega_m < 0.5$? Is $\Omega_\Lambda \neq 0$?

3 Clusters: The Place to Be and Be Seen

Our view of the Universe traditionally has been baryon-biased: we see or detect luminous objects. Yet for the past 15 years it has become more certain that the Universe is dominated by non-baryonic dark matter.[2,9] Of course, luminous objects, through their dynamics, can supply indirect estimates of the local underlying mass. On very large scales, our currently favored notion of hierarchical structure formation predicts that mass and light should be correlated.

As overdense regions in the Universe grow, some of them become sufficiently overdense that they "freeze out"; inside some radius they overcome the expansion of the Universe. As their density rises into the non-linear regime, their internal density fluctuation spectrum bears little resemblance to the primeval spectrum. However, it is hoped that at least the matter *content* of clusters is representative of the Universe. It is probably too much to hope that their mass-to-light ratio is also representative. Traditionally, clusters have been found via their radiation (optical light or X-ray). Until recently, the masses of galaxy clusters have played a central role in our understanding of dark matter problems.

Cluster masses can be estimated by three different techniques which, on scales of 1 Mpc, give consistent results. The first, which dates back to Zwicky (1933), uses the measured velocities of cluster galaxies and the virial theorem to determine the total mass (i.e., $KE_{\rm gal} \simeq |PE_{\rm gal}|/2$). Assuming further that the mass-to-light ratio of clusters is the same as the mean mass-to-light ratio in the Universe, one can combine measurements of the dispersion of velocities of hundreds of galaxies in several clusters with a measurement of the mean light density to arrive at an estimate of the mean mass density[10]: $\Omega_M \approx 0.25$. If clusters have more luminosity per mass than average, this technique would underestimate Ω_M.

The second method uses the temperature of the hot X-ray emitting intracluster gas and the virial theorem to arrive at the total mass. In this method, one must assume that the hot gas is pressure supported and in equilibrium. The density and temperature profiles of the hot gas must also be obtained. Often temperature is not mapped, so isothermality is assumed when inverting flux maps to get the potential.

The third and most direct method is utilizing the gravitational lensing effects of the cluster on much more distant galaxies. Light from distant galaxies scatters off the mass gravitationally. For small impact parameters, close to the cluster center, lensing is strong enough to produce multiple images. Farther out, lensing distorts the shape of distant galaxies. The lensing method allows the cluster surface mass density to be mapped directly. [In the following I will use h, the Hubble constant in units of 100 km s^{-1} Mpc^{-1}. Recently, h has been measured[11] to 10% accuracy, $h = 0.67 \pm 0.1$.]

X-ray measurements more easily determine the amount of hot, intracluster gas; most of the baryonic mass in a cluster resides in this form rather than in the mass of individual galaxies (this fact is also confirmed by lensing measurements). If we can assume that clusters are fair samples of matter in the Universe, we can use baryogenesis to get an indirect estimate of Ω_M. Together with the total cluster mass, the ratio of baryonic mass to total mass can be determined; a compilation of the existing data[13] gives $M_B/M_{\rm TOT} = (0.07 \pm 0.007)h^{-3/2} \sim 0.15$. Invoking the "fair sample" ansatz $\Omega_B/\Omega_M = M_B/M_{\rm TOT}$, the accurate BBN determination of Ω_B can be used to infer: $\Omega_M = (0.3 \pm 0.05)h^{-1/2} \sim 0.4$.

Traditional methods of estimating total mass of clusters are indirect: mass estimators based on kinematics or X-ray flux maps involve models of orbits or the

state of the hot gas, leading to possible systematics in the derived gravitational potential. While the dynamical evidence for dark matter is strong on scales from galaxies to superclusters of galaxies, it is worthwhile exploring independent observational techniques which do not rest on assumptions about the orbits of test particles. But luminous clusters may be a biased sample.

There are two ways in which confining the study of mass to clusters may lead to a biased measure of the mass content of the Universe. First, the mass-to-light ratio within the cluster may not be typical; i.e., a higher baryon fraction may lead to more light per mass. Second, being selected because of their luminosity, clusters may be a statistically biased sample of mass. If we examine other regions in equal detail, we will be able to examine this possibility.

4 Introduction to Lensing

Gravitational lens distortion of background galaxies enables calibrated measurements of the distribution of dark matter in the Universe. This lens phenomenon is most naturally divided into two broad classes: strong lensing and weak lensing. In weak lensing the gravitational deflection angles are very small and single sources produce single (but distorted) images. In strong lensing, sources appear highly distorted and can form multiple images. Whether a given source is weakly or strongly lensed depends on the impact parameter of the ray: whether its image appears outside or inside the critical "Einstein" radius. For an excellent lensing tutorial, see Narayan and Bartelmann.[12]

The large number of potential sources in the wide area outside the critical radius of a foreground lens offers the possibility of statistical tomographic reconstruction of the mass distribution in the outer parts of the lens. This weak gravitational lensing provides a direct measure of mass overdensity on a variety of scales (several kpc to tens of Mpc, depending on the distance and compactness of the lens).

Strong lensing analysis constrains the mass distribution in the parts of the lens which exceed the critical density for image splitting. In cases where multiple images of a source are created by the lens, the details of the position and distortion of these sub-images are highly sensitive to the projected two-dimensional mass distribution within the lens.

In weak lensing it is necessary to average over the apparent orientation of tens of sources for each mass resolution element: typically, weak lens statistical inversion uses tens of thousands of "arclets" (distorted background galaxies) over a wide field.[14,15] The largest source of noise in weak lens inversion of deep optical images is the ellipticity noise of the source population itself; galaxies are not round and they come in all orientations. A number of non-parametric algorithms have been developed for inverting the arclets, and regularized approaches have been developed to avoid edge effects and systematics near the strong lens regime.

Up to a constant sheet of mass, lensing inversion can be calibrated and has no adjustable parameters. Calibration of the mass scale can be done both through simulations and via observation of a mass standard. Realistic simulations of the whole source-lens-atmosphere-detector process must be performed, including multiple background galaxy redshift shells, masses for individual cluster galaxies, dark matter lens model, atmospheric seeing, and pixel sampling and sky shot noise. "Blank" field Hubble Space Telescope imaging data, together with seeing deconvolved ground-based data, are used to derive the source galaxy angular scales. Mass calibration via strong lensing forms an independent check on weak lensing mass scale calibration. There are now many of these mass calibrator clusters over the sky; the redshift of the arc is known so that the mass enclosed with that radius is known. Through comparison with large N-body simulations for various cosmogonies, this new window on mass in the Universe constrains the nature of dark matter.

5 The Sources

To 30th magnitude per square arcsecond surface brightness (4×10^{-18} erg sec^{-1} cm^{-2} arcsec^{-2} in 100 nm bandwidth at 450 nm wavelength, or about five photons per minute per galaxy collected with a four-meter mirror), there are about 50 billion galaxies over the sky. Nature has been particularly kind to us: Since many of the faint galaxies are resolved and are distributed up to high redshifts, they may be employed in statistical gravitational lens studies of foreground mass distributions. As we will see, if galaxies were a few times smaller or less luminous in the past, this "cosmic mirage" would be extremely difficult to use. For mass mapping by statistical gravitational lens inversion, the sources must meet several requirements: The sources must have (1) redshifts large compared with

the lens, (2) a number density on the sky sufficient to sample the lens shear field on relevant scales, (3) an intrinsic angular diameter larger than the ratio of seeing FWHM to the magnification of the lens (i.e., we must be able to detect the image distortion), and (4) other properties (blue color and unique surface brightness) enabling efficient separation of the sources from superimposed galaxies within the lens and foreground.

The extreme blue colors of the faint galaxies results from their large look-back times: we see these young galaxies as they were billions of years ago just forming a generation of hot and UV-bright stars at redshifts of 1 to 3, so that their UV excess flux is redshifted into the blue. In a redshift-magnitude plot of hundreds of galaxies, the trend to redshift ~ 1 at 25th B magnitude is clear. A typical galaxy seen at $z = 1$ may be a 0.1 L^* galaxy, so a survey at 25th magnitude would cover a wide range in redshifts extending from 1 to 3. For arclet inversion of $z < 0.3$ lenses, the lack of detailed redshift data for each of these sources produces less than a 10% mass scale error. We can do even better: if deep imaging is done in several wavelengths, there is enough low resolution spectral information to supply so-called "photometric redshifts," accurate to $\Delta z = 0.1$, so we can separate galaxies into broad foreground and multiple background redshift bins. This raises the lens inversion signal-to-noise level. The number density of galaxies on the sky vs magnitude is shown in Figure 3.

Without luminosity evolution these distant background galaxies would have prohibitively faint surface brightness ($SB \sim (1+z)^{-4}$). Even with their luminosity evolution (brighter earlier), very faint levels of surface brightness must be achieved. This is the most difficult part of this technique, and is why many orbits on HST or several nights on large ground-based telescopes are required per field in order to achieve good signal-to-noise imaging in several wavelength bands. At any surface brightness limit, there is a redshift selection function, as shown in Figure 4. Two limiting surface brightnesses are used in this simulation of the number count vs redshift of 25-26th magnitude galaxies: 29 mag arcsec^{-2} (typical of four hours of large ground-based telescope CCD exposure) and 26 mag arcsec^{-2} (typical of several orbits of the HST CCD). As may be seen, there is a huge increase in the number of galaxies behind a redshift 0.5 lens by going from 26 to 29 surface brightness (or about ten photons per minute per galaxy collected with a four-meter mirror). The largest background is the Poisson noise from the "dark" no-moon night sky diffuse light (mostly low level aurora) at a surface brightness of about

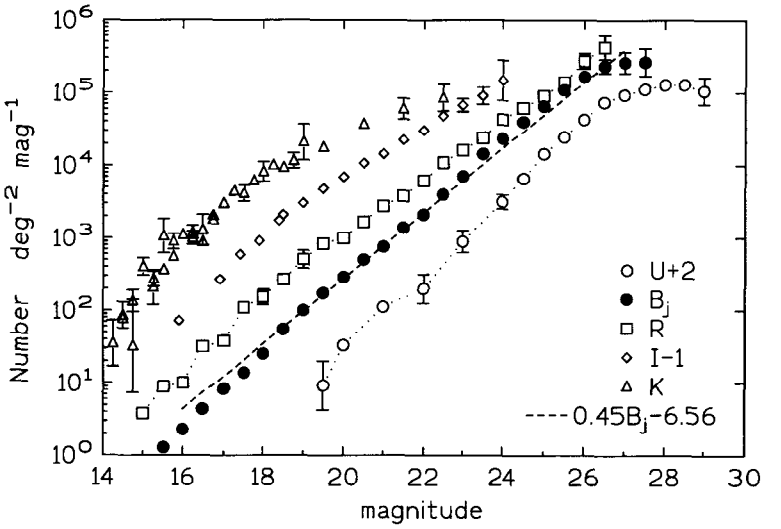

Fig. 3. Number density of galaxies (the sources) on the sky, as a function of magnitude (-2.5 log flux) for several wave-bands, U (360 nm), Bj (450 nm), R (600 nm), I (800 nm), and K (1200 nm). There is a faint galaxy every few arcseconds on the sky, in deep imaging on large telescopes, sufficient to define the shear field of a foreground gravitational lens.

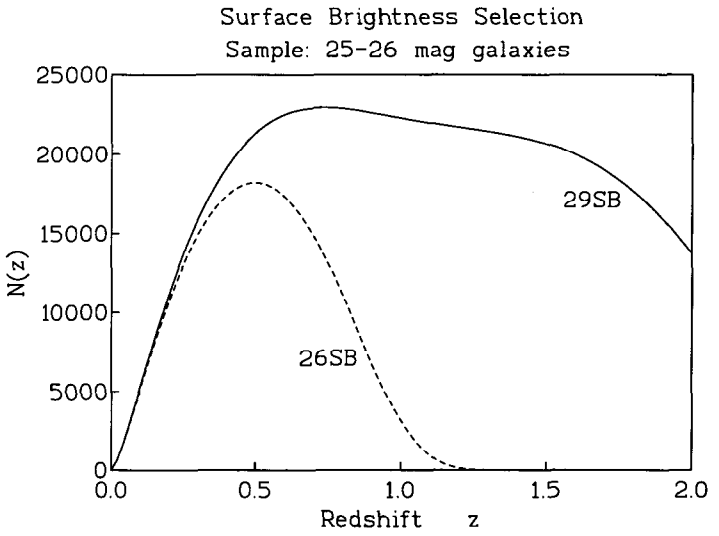

Fig. 4. The effects of a surface brightness limit on the distribution of redshifts found in a simulated survey of 26 magnitude galaxies. Due to the Hubble expansion, higher redshift galaxies appear to have fainter surface brightness, thus systematically dropping out of a surface brightness limited sample. In this simulation, the higher star formation rate of galaxies in the past was taken into account.

23 mag arcsec^{-2} at 400 nm, rising by a factor of three at red wavelengths.

Galaxies fainter than 26 B magnitude also cover a wide range of angular scales; typical half-light diameters are 1 arcsecond.[16] Image quality is critical; galaxies of less than 1 arcsecond diameter must be resolved, in order to measure their ellipticity. Four- to six-meter class telescopes can image one square degree to a magnitude limit of 27 B (blue) mag and 29 B mag arcsec^{-2} surface brightness in several nights per wave-band. Sufficiently deep multi-wavelength imaging can provide the input data for studies of mass via gravitational lensing.

6 Light Bending

The path of a photon from a distant source is bent as it passes by the foreground mass (gravitational lens), making the source appear at an altered position (for a good review, see Ref. 17). This light-bending is accompanied by another first-order effect: systematic image distortions. If the background source image is resolved, then this image stretching is observable. A galaxy of angular size one arcsecond may appear to be moved by an angle $\beta = 4GM(r)/rc^2$ and distorted into an arc many arcseconds long by sufficient foreground mass $M(r)$ interior to projected radius r. The scattering time is small compared with the period of orbiting test particles, thus avoiding orbit assumptions.

The light deflection is proportional to the mass in the lens and is about two arcsec for a typical galaxy.[18] If ϕ is the intrinsic source position in the absence of the lens, the observed source appears at position θ:

$$\vec{\phi} = \vec{\theta} - \vec{\delta}(\vec{\theta}), \tag{1}$$

$$\vec{\delta}(\vec{\theta}) = (D_{LS}/D_S)\ \vec{\beta}(\vec{r}),$$

where r is the impact parameter for the ray at the lens, and D_S and D_{LS} are the observer-source and lens-source angular diameter distances. For a thin lens the light bending angle $\vec{\beta}$ is given in terms of the projected two dimensional mass density Σ:

$$\vec{\beta} = (4G/c^2) \int d^2u\ \Sigma(\vec{u})\ (\vec{r} - \vec{u})\ /\ |\ \vec{r} - \vec{u}\ |^2\ . \tag{2}$$

We would like to invert this relation and solve for the mass density $\Sigma(x, y)$. Since we do not know how the sources were distributed on the sky prior to lensing, this deflection itself is not observable. But its gradient, the shear, is directly observable. In the simple case of a pont mass, $\beta = 4GM/rc^2$, so a source exactly behind the mass appears as an "Einstein ring" image of radius $\theta_E = (M\ /\ 10^{11}\ M_\odot)^{1/2}\ (D\ /\ 10^6\ \mathrm{kpc})^{-1/2}$ arcseconds, where $D = D_L D_S/D_{LS}$. If the lens mass is elliptical in shape or has multiple mass components, this circular ring symmetry is broken, so that in nature circular rings are rare. If the source angle ϕ is less than θ_E, then multiple images of the source are formed. Galaxy lenses ($M \approx 10^{12}\ M_\odot$) will produce multiple images with separations ≈ 3 arcseconds,

while galaxy cluster lenses ($M \approx 10^{14}\ M_\odot$) can produce image separations of one arcminute. Astronomers often use velocity dispersion as a proxy for mass: for an isothermal distribution $M/r \sim v^2$ is independent of r. In the case of an isothermal distribution of gravitationally bound masses of line-of-sight velocity dispersion σ_v, $\beta(r) = 4\pi(\sigma_v/c)^2$, $\theta_E = 29\ (\sigma_v\ /\ 10^3\ \mathrm{km\ sec^{-1}})^2\ (D_{LS}/D_S)$ arcseconds. Many clusters have measured velocity dispersions $\approx 10^3$ km sec^{-1}. Most have $\sigma_v \approx 700$, and a few have $\sigma_v \approx 1500$ km sec^{-1}. As an aid in understanding the observational consequences of gravitational lensing, particularly strong lensing, it is useful to visualize the effects of such a massive cluster in a movie of 1000 realizations of lensing.

6.1 Simulation Movies

MPG MOVIES of our view, over the next few billion years, of a cluster of galaxies and the effects of its dark matter are shown in
"`ftp://netlib.bell-labs.com/cm/physics/who/tyson/MPEG/LENS0.mpg`"
and
"`ftp://netlib.bell-labs.com/cm/physics/who/tyson/MPEG/LENSMAX.mpg`".
These simulations were made by our group, principally Ayana Holloway. They show the cluster A1689 as viewed by Earth orbiting space telescopes over the next few billion years; as it moves through the Universe its alignment with the background faint blue galaxies constantly changes. The data for the cluster (the orange bright galaxies) are from the Hubble Space Telescope, and the mass model is one which we are developing for this particular cluster, based on very deep multi-color HST and ground-based imaging of A1689, via strong lens parametric techniques. (For a description of parametric strong lens mass determination, see Tyson, Kochanski, and Dell'Antonio.[19])

These first two movies are based on two extreme mass models: LENSMAX.mpg has much of the mass in the halos of the cluster galaxies, while LENS0.mpg has very little mass in the cluster galaxies (most mass residing in a single dark mass).

The background galaxies are placed in six redshift sheets, out to $z = 3$. Fainter and bluer galaxies are at higher redshift. Some galaxies just behind the cluster (coded brighter and less blue) are only slightly distorted by the concentration of dark matter. The highest redshift faint galaxies easily form large arcs (perturbed Einstein rings) at larger radii.

Our mass distribution is composed of dark matter halos for individual cluster galaxies as well as the dominant diffuse mass of the cluster. This largest mass has a soft core. A non-singular lens mass produces an odd number of images of a background galaxy. When the galaxy is at large projected radius (weak lens regime) it is slightly distorted orthogonal to the radius vector. As the galaxy moves into the critical region, it splits into an odd number of images, usually two arcs on opposite sides of the lens and a third, demagnified image near the center. The details of these images—their parity and magnification—are sensitive to the gradient of the lens mass. For regions near the core where the lens mass density exceeds the critical mass density, the magnification determinant is negative—the lens-focused light bundle comes to a focus before reaching Earth. Images inside this radius (one of the odd images) appear demagnified and with opposite parity. These faint radial spokes may be seen for many of the background galaxies over a finite range of impact parameter, and are a sensitive indicator of the size of the soft mass core. Another observed feature of our lens model for this cluster is the unusually thin arcs (images of high-z galaxies); this is due to a mass profile which is steeper than isothermal.

We spent some effort to mpeg encode these movies in a way that is maximally compatible with Windows and Unix mpeg players. If you experience problems, please let us know. We use MPEG-1 format.

7 Tomographic Reconstruction of Galaxy Cluster Mass

7.1 Weak Lens Statistical Inversion

Historically, the first solution to this inverse problem was via statistical weak lens inversion, in which the mean shear field is estimated from the tangential alignment of stretched single images of many independent background galaxies projected near the cluster.[15] It was logical to apply this new technique first to massive clusters where there was already indirect evidence for a high mass contrast. Weak lens statistical inversion still plays a dominant role in most gravitational lens examinations of cluster mass, since few clusters have the unlikely favorable alignment with a background source that gives rich multiple images of that single source. Pedagogically, however, strong lensing presents a striking demonstration of the

effects of lensing, as seen in the above movies. In principle, strong lensing also gives higher resolution mass maps than statistical weak lensing. I postpone discussion of the more generally useful technique of statistical weak lensing to a later section.

7.2 Strong Lens Parametric Mass Models

Multiple images of the same resolved source galaxy contain rich information related to the mass distribution in the lens. In cases where portions of the lens exceed critical density, producing multiple images of some sources, it is possible to obtain higher resolution in the mass map by combining weak lens inversion at large radius with the strong lensing constraints in the inner region. There are perhaps a few hundred moderate redshift clusters which have super critical core densities, and some of them have the chance alignment required to give obvious multiple resolved images of a bright single source. One approach is to use a parametric lens model in which multiple mass components are parametrized by their centroid, mass profile, and ellipticity. An iterative approach, regularized by the weak lens inversion solution for the mass at large radius, may then be used to obtain a unique solution for the lens mass map at high resolution.

This has the desirable property that the resulting mass map has high resolution in regions of high mass density. In practice we have found that a reliable way of converging to the solution is to demand that the strong lensed source images, when unlensed by the estimated mass distribution in the lens, reconstruct to an identical single image,[20] and that this image of the source maps to the observed arcs (and only these arcs!) in the image plane when lensed by this same mass. It is necessary to use the lens *mass* distribution, rather than the approach of starting with a two-dimensional lens potential, because non-circular lens potentials can be unphysical in their corresponding mass reconstructions.

With my colleagues Ian Dell'Antonio and Greg Kochanski, we have developed a code for this weak-strong mass reconstruction and applied it to complex lens simulations as well as deep HST imaging of two massive clusters, the first being the $z = 0.4$ galaxy cluster CL 0024+17. The projected mass density contrast at large radius is obtained from over a thousand arclets, excluding the bright long arcs, in a wide field using a ground-based telescope. The mass density contrast at intermediate radius (up to two arcminutes) is obtained from weak lens inversion of 350 arclets found in the HST deep images. Finally, the mass map in the inner region is reconstructed from the multiple strongly lensed images of a single source galaxy via the procedure outlined above.

As an example, Figure 5 shows a high resolution mass map of the $z = 0.39$ cluster 0024+1654, based on parametric inversion of the associated gravitational lens.[19] This lens creates eight well-resolved whole or partial sub-images of a background galaxy, seen in deep imaging with the Hubble Space Telescope.

Of course we do not know what the source galaxy looks like; so we cannot start with that prior. The source galaxy optical image must be part of the model to be optimized along with the mass distribution in the lens. We parametrized the source as 58 smooth disks of light. Each of these disks was characterized by an intensity, a scale radius, and the (x, y) position on the source plane (four parameters). A source plane resolution of seven milli-arcseconds per pixel was chosen to allow sufficient evaluations of the model to be done within a reasonable time (12 months), and to allow the model to represent almost all details of the observations. The source is then ray-traced through the lens plane, and the resulting image is compared on a pixel-by-pixel basis with the HST image. We parametrize the mass distribution as a cluster of mass concentrations ("mascons"). Each mascon is based on a power law model[21] ("PL"), for the mass density $\Sigma(r)$ vs projected radius r, with both an inner core radius and an outer cutoff radius

$$\begin{aligned} \Sigma(x) &= \frac{K_1(1+\alpha x^2)}{(1+x^2)^{2-\alpha}} \qquad x < X_o \\ \Sigma(x) &= K_2 x^{-3} X_o^3 \qquad x \geq X_o, \end{aligned} \tag{3}$$

where $x = r/r_{\rm core}$, $X_o = r_{\rm cutoff}/r_{\rm core}$, and α is the PL model index. ${K_1}^{0.5}$ is proportional to the central line-of-sight velocity dispersion. We build up elliptical mass distributions by superposing a line of overlapping circular mascons. In principle, each mascon is described by nine parameters, although most do not require more than a few parameters. The first four come directly from the equation above (K_1, an inner mass core radius $r_{\rm core}$, an outer mass cutoff $r_{\rm cutoff}$, and the slope of the mass profile α). For elliptical mass distributions, there are three parameters describing the ellipticity (the position angle θ, the length of the line of mascons l_{core}, and the uniformity of the spacing of the mascons along the line). For mass components not associated with optically observed galaxies, the x and y position in the lens plane are also free.

The mass and linear scale sensitivity of this parametric lens inversion technique vary with position in the cluster; cluster mascons projected near a long arc have the effect of their mass distribution highly magnified. For galaxies that are more than about five arcseconds from the arcs, only their total mass matters, and we parametrize this by the cutoff radius (because $M \propto r_{\rm cutoff}$). Galaxies farther than about 20 arcseconds from the arcs are parameterized in groups.

In all, the mass and source models are determined by 512 parameters. However, we have over 3800 significantly nonzero (3σ) pixels in the arcs which supply sufficient information. Because the optical point spread function of the WFPC2 is smaller than one pixel, the signal is nearly uncorrelated even on neighboring pixels; thus, we have many more independent constraints than model parameters. In addition, pixels with no signal serve as constraints, because they prevent the model from putting flux in areas of the image where there is none. The resulting mass model is over-constrained. The optimizer uses simulated annealing and bootstrap resampling to avoid false minima.

As we developed the model, it had enough power to predict the central image, based on the three major arcs, then to correctly predict the multiple subimages near the outer arcs. One of these was buried under a cluster galaxy and was recovered as a result of this prediction by modeling and subtracting the foreground galaxy's light. The galaxy masses in the model were initialized using the Faber-Jackson relation between a galaxy's optical luminosity and mass. When the model evolved to a low χ^2, we performed robustness tests by multiply perturbing the position and/or mass of mascons and observing the reconvergence to the solution (see Figure 5). Over 2×10^6 models were searched to reach the solution. In addition to the large diffuse mascons, other mascons were added to our fit to allow it to match the complexity of the cluster's mass distribution. Several "dark" galaxies were found.

The vast majority of the dark matter is *not* associated with the galaxies, and appears as a smooth elliptical distribution centered near the position of the brightest galaxy and elongated in the SE-NW direction. The elongation is in the same direction as that of the X-ray isophotes. This dark matter not associated with galaxies shows no evidence of infalling massive clumps: other than these two major clumps, we find no dark mascons with total mass greater than $5 \times 10^{12} M_\odot$ (1.5% of the cluster mass), out of the 25 in the fit.

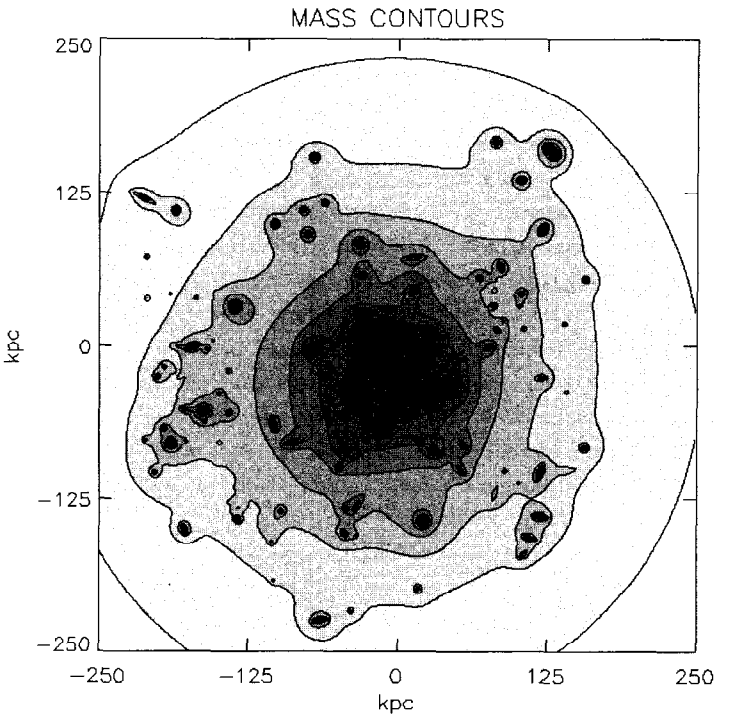

Fig. 5. A map of the projected mass density in the redshift 0.4 cluster CL0024+1654, obtained by fitting the observed distorted images of a $z = 1.6$ source galaxy. Dark matter halos of individual galaxies in the cluster are seen, but the major dark matter component is relatively smooth compared with CDM simulations.

Excluding mass concentrations centered on visible galaxies, more than 98% of the remaining mass is represented by a smooth concentration of dark matter centered near the brightest cluster galaxies, with a 33 h^{-1} kpc *soft core*. The asymmetry in the mass distribution is <3% inside 107 h^{-1} kpc radius. The dark matter distribution we observe in CL0024 is far more smooth, symmetric, and nonsingular than in typical simulated clusters in either $\Omega = 1$ or $\Omega = 0.3$ CDM cosmologies. Integrated to 107 h^{-1} kpc radius, the rest-frame mass to light ratio is $M/L_V = 238 \pm 16\ h\ (M/L_V)_\odot$, rising with radius (see Figure 6). Because galaxies were brighter in the past, this translates to a mass-to-light ratio of 400 h now. For scale, we would need around 1200 to extrapolate to $\Omega_M = 1$.

The mass distribution in CL0024 is remarkably relaxed. If one assumes Gaussian density fluctuations in an $\Omega = 1$ Universe, the fluctuation that seeded CL0024 must have had a very large amplitude quite early (rare) to have become virialized by $z = 0.39$. One is led to consider non-Gaussian fluctuations or $\Omega << 1$. An important open question is whether galaxy cluster formation is still continuing at recent times. That is, do a significant fraction of galaxies fall into a pre-existing deep cluster potential? Given that galaxies are detected at redshifts as high as 4, simple top-down (large scales first) structure formation is ruled out. But there may be several components to the mass-energy of the Universe, and thus multiple contributors to the density profile of clusters.

A key result of this first high resolution mass map is the existence of a 33 h^{-1} kpc soft core. Any possible singularity must be quite small, contributing less than $2 \times 10^{11}\ h^{-1} M_\odot$ to the total mass within 33 h^{-1} kpc (10% of the mass of one of the central elliptical galaxies). Because cold collisionless particles have no characteristic length scale, the soft core suggests either nongravitational interactions or gravitational coupling to a dissipative baryonic component of significant mass fraction. While HDM can produce soft cores, HDM is not consistent with the high density of dark matter that we find in the individual cluster galaxies. Because of the relatively low X-ray luminosity (0.7 L_X^*), it is unlikely that this can be attributed to hot gas alone.

High resolution mass maps of clusters of galaxies will be useful to compare with future N-body/gas-dynamical simulations. None of the recent simulations show evidence of a soft core, in disagreement with these observations. Indeed, as the resolution of simulations increases from 100 to 30 kpc the central mass becomes more singular.[22] At this time it is too early to conclude whether this

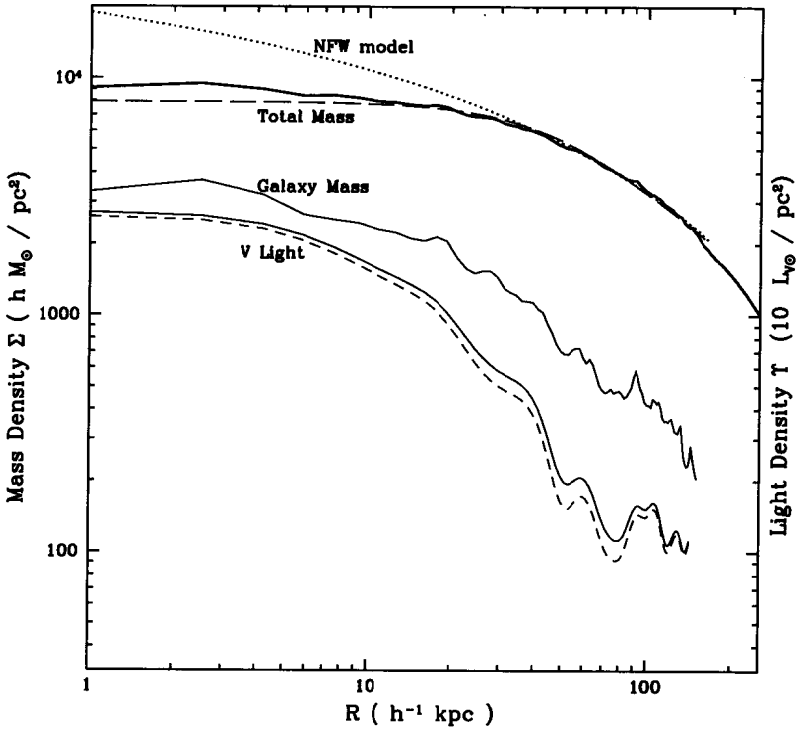

Fig. 6. The projected mass density of CL0024 and the projected light density are plotted vs radius. The diffuse dark matter component dominates, and has a soft core. Note also that the mass-to-light ratio rises with radius.

soft mass core is a result of baryon interactions or a feature of non-baryonic dark matter. Another technique, the Sunyaev-Zel'dovich effect, which makes use of the Compton up-scattering of CMB photons when viewed through a cluster containing hot gas, may soon prove helpful in resolving this question. While the angular resolution achievable in this CMB decrement imaging is lower than the strong lens inversion maps, "SZ" imaging of the projected hot gas density depends on redshift and other cosmological parameters in the same way as gravitational lens mass imaging, so that the cluster gas to total mass ratio may be derived directly from the combined lens/SZ data.

8 Statistical Weak Lensing

If the source angle relative to the lens ϕ is larger than θ_E, multiple images of a source will not be formed, but the single image of the source will be elongated as shown in Figure 7. Since there are roughly 100 independent resolved sources per square arcminute, this enables a different kind of solution to the inverse problem, called "statistical weak lensing." This method has the advantage that it is generally applicable, and gives good signal-to-noise inversions in regions of low shear which are much more representative of random regions.

The huge mass associated with clusters of galaxies distorts all the background galaxies many arcminutes from the cluster. Foreground galaxy clusters at redshifts 0.2(0.5) with radial velocity dispersions above 700 km sec^{-1} have sufficient mass density to significantly distort background galaxies of redshift greater than 0.4(1). Lensing preserves the surface brightness and spectrum of the source, so that arcs tend to have the very faint surface brightness and blue color of the faint blue galaxies. A simulation of both weak and strong lensing is shown in Figures 8 and 9. First, a long cone is populated with galaxies of size and luminosity appropriate to their epoch, out to redshift 3. Then a cluster mass is placed at redshift 0.3, distorting the images of these background galaxies.

8.1 Inverse Problem: Mass from Image Distortion

This gravitational lens distortion is quantified using the intensity-weighted second moment of the galaxy image orthogonal and along the radius relative to the lens center.[15] A dimensionless scalar alignment T, calculated from these principle axis

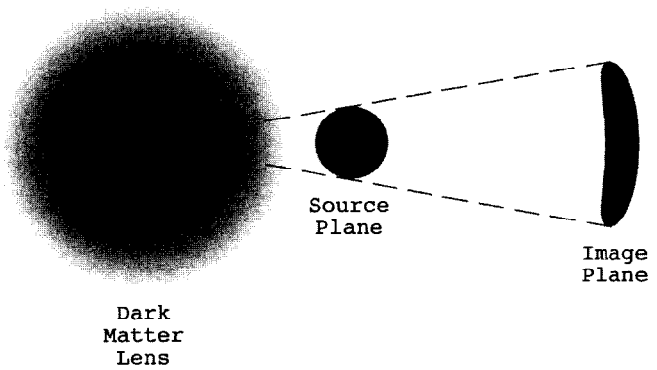

Fig. 7. Resolved background galaxies (source plane) are mapped into distorted images (image plane) by the light bending due to the foreground mass (left).

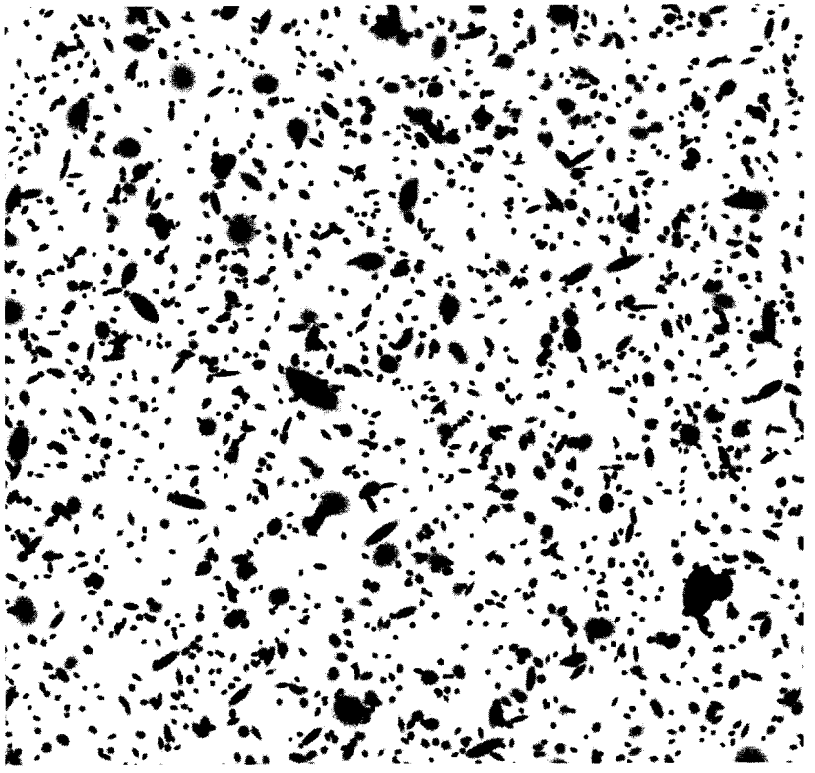

Fig. 8. A view of the sky, several arcminutes wide, looking through the forest of galaxies out to redshift 3. This simulation was made to simulate Hubble Space Telescope deep imaging data. No large dark matter concentration (lens) was included.

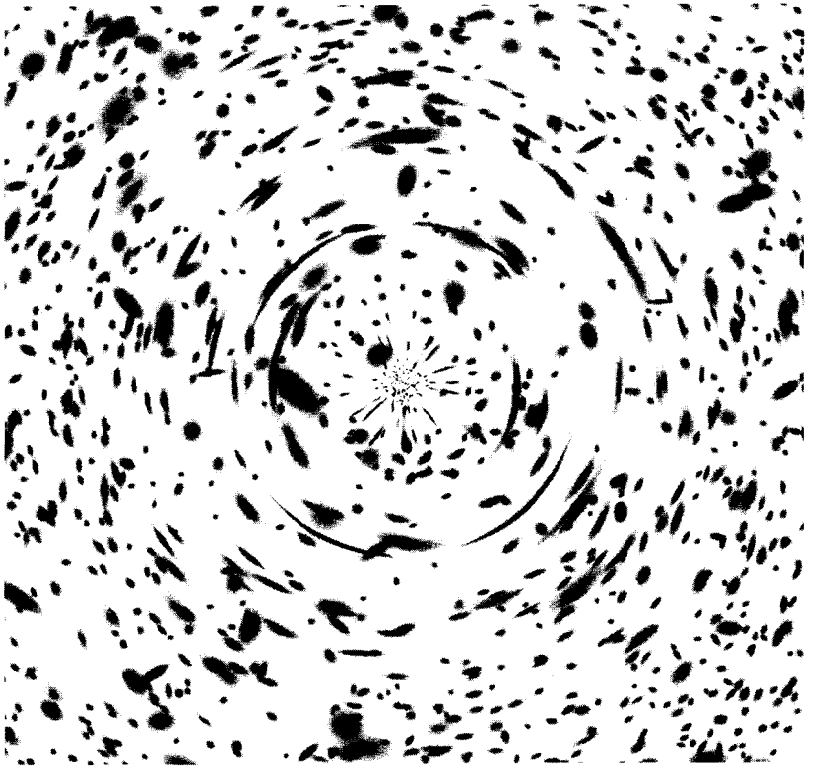

Fig. 9. The effects of a dark matter concentration of the type found in rich clusters of galaxies on the simulated sky shown in the previous figure. Foreground galaxies are unaffected; background galaxies are increasingly distorted at higher redshift. Both strong lensing (large arcs, some multiple images of a single source) and weak lensing (mildly distorted single source galaxy image) are seen. The radial spikes close to the center are a diagnostic of a soft mass core.

transformed source ellipticities, is related to the projected mass density clumping, and is defined at each point $(\vec{r})$ in the image plane via the (r, θ) principal-axis transformed second moments of the background galaxy image:

$$T(\vec{r}) = \frac{i_{\theta\theta} - i_{rr}}{i_{\theta\theta} + i_{rr}} = \frac{2(1-\kappa)\gamma}{(1-\kappa)^2 + \gamma^2} \simeq \frac{2\gamma(\vec{r})}{1-\kappa(\vec{r})}, \tag{4}$$

where the convergence[23] $\kappa(r) = \Sigma(r)/\Sigma_c$ and the shear $\gamma(r) = [\bar{\Sigma}(r) - \Sigma(r)]/\Sigma_c$, and where Σ_c is the critical surface mass density, related to the distance ratio: $\Sigma_c = c^2/(4\pi G D)$. The distance ratio for a foreground-background pair is[17]

$$D = \frac{(1 - q_o - d_1 d_2)(d_1 - d_2)}{(1 - q_o - d_2)(1 - d_2)(1 + z_{fg})}, \tag{5}$$

where $d_1 = \sqrt{1 + q_o z_{fg}}$ and $d_2 = \sqrt{1 + q_o z_{bg}}$.

Introducing a galaxy light distribution prior, the tangential second moments are

$$\begin{aligned} i_{\theta\theta} &= M_{20} \sin^2\phi + M_{02} \cos^2\phi - 2M_{11} \sin\phi \cos\phi, \\ i_{rr} &= M_{20} \cos^2\phi + M_{02} \sin^2\phi + 2M_{11} \sin\phi \cos\phi, \end{aligned} \tag{6}$$

where ϕ is the position angle of the vector from the point (x, y) to the background galaxy, relative to the x-axis. The intensity-weighted second moment $M_{lm,g}$ of the background galaxy g is defined by

$$M_{lm,g} = M_{0,g}^{-1} \int (\delta x)^l \, (\delta y)^m \, W(\delta x, \delta y) \, [I_g(\delta x, \delta y) - I_0] \, dx \, dy, \tag{7}$$

$$M_{0,g} = \int W(\delta x, \delta y) \, [I_g(\delta x, \delta y) - I_0] \, dx \, dy,$$

where $\delta x = (x - < x >_g)$ and similarly for δy; the sky intensity near this background galaxy is given by I_0, and optimal normalized Gaussian weights (adaptive kernel) $W(\delta x, \delta y, I(x, y))$ are calculated from the half luminosity radius. An unlensed population of galaxies randomly placed and oriented will give a net distortion $T(\vec{r})$ of zero at every point in the image plane, while a population of lensed galaxies will give a positive value at the point corresponding to the lens center. At some point off the lens center $T(\vec{r} - \vec{r}_0)$ is proportional to the projected mass at that new point, as shown in Figure 10.

In three-dimensional simulations of deep shear surveys, it is apparent that in addition to the shear noise arising from intrinsic source galaxy random ellipticities there are errors arising from occasional chance projections of one arclet very near

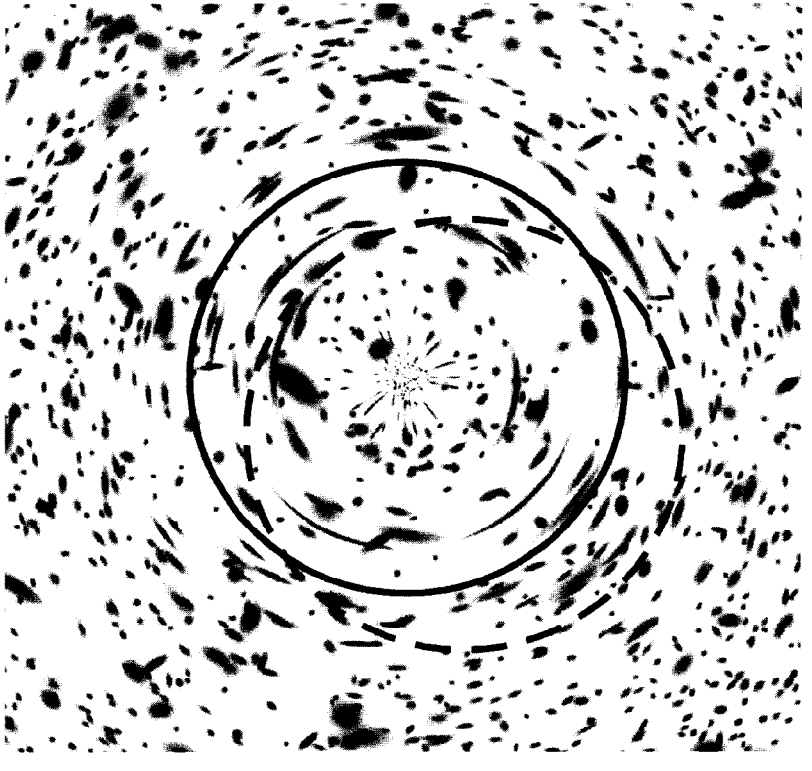

Fig. 10. The sum of the tangential component of the shear around the solid circle is simply related to the average mass density interior. This is also true for the offset (dashed) circle. This provides a method for mapping the projected mass density on the sky, producing images of the dark matter. The resolution is given by the size of the circle. In practice, a weighted average of an array of sizes is used in deriving the mass map.

or on top of another. We have found that a regularized iteration, in which the kernel $W(\delta x, \delta y)$ is elliptical and the maximum likelihood is matched to each arclet, is even more effective in reducing the tail of the arclet ellipticity noise.

9 Cluster Mass Distribution from Arclets

To construct an image of the gravitational lens projected mass distribution, the distortion statistic $T(\vec{r})$ may be computed over a grid of positions as candidate lens centers. In the weak lensing limit it can be shown that the tangential alignment T is a measure of the mass contrast:[14,23]

$$T(\vec{r}) \;=\; 2\,[\Sigma_{av}(<r) - \Sigma(r)]\;\Sigma_c^{-1}. \tag{8}$$

At any point $\vec{r}$ in the image plane we can sum over the tangential alignment of all source images about that point, creating a continuous scalar distortion statistic $\bar{T}$:

$$\bar{T}(\vec{r}) = \int K(\vec{u})\; T(\vec{r} - \vec{u})\; d\vec{u}, \tag{9}$$

where the apodization kernel $K(\vec{u})$ weights source images at large radius less, and is generally of the form $K(\vec{u}) \;=\; (u^2 \;+\; u_0^2)^{-1}$. For $\bar{T}$ to be simply related to the mass[24] $K(s)$ must asymptotically approach the power law s^{-2} at large s. The distortion $\bar{T}$ at any point is related to the mass density contrast, since any mass can be represented as a sum of cylindrically symmetric distributions, and light bending angles from different mass components add. The solution to this inverse problem for the contrast of the projected lens mass density Σ is then given by a simple integral of the shear over the radius from the lens center. The average projected mass density interior to radius r is given by

$$\bar{\Sigma}(r) \;=\; \Sigma_c C B(r) \int_r^{r_{\max}} T(r)\; dlogr \;+\; \bar{\Sigma}(r, r_{\max}), \tag{10}$$

where C is the seeing correction, obtained via simulations. The function B is given by $B(r) = (1 - r^2/r_{max}^2)^{-1}$, and $\bar{\Sigma}(r, r_{max})$ is the average density in the annulus between r and $r_{\max}$. For a sufficiently large field, $\bar{\Sigma}(r, r_{max})$ is small compared with peak density. This arclet inversion is called "aperture mass densitometry." No map is obtained; just the radial profile. A radial plot of the projected surface mass density found using Eq. 10 is shown in Figure 11 for $z_l = 0.3$, $\sigma_v = 1000$ km sec^{-1} simulations with two different mass profiles.

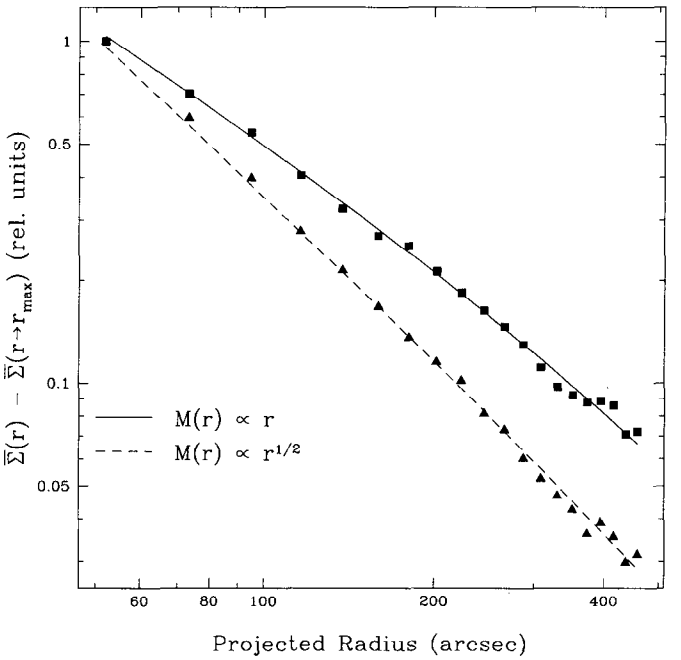

Fig. 11. A radial plot of the projected mass density contrast obtained by inversion of the arclets in two 29 B mag arcsec^{-2} noisy simulations of a cluster of galaxies dominated by dark matter with velocity dispersion $\sigma_v = 1000$ km sec^{-1}. Two test mass distributions are shown, arbitrarily normalized at 50 arcsec radius. The lines are the input mass density functions.

The distortion image $\bar{T}(x,y)$ uniquely locates the lens mass, obtains $M(<r)/r$, and gives its morphological shape on the sky. A useful check of this procedure uses the mass map (Eq. 9) as input to a Bayesian search in model mass distribution space, solving for the dark matter mass and core size. For the known source ellipticity distribution, a given source redshift distribution, and a test radial mass distribution model, a maximum likelihood calculation yields the lens M/r (or equivalent velocity dispersion) and core radius. From the inversion of 6000 arclets surrounding the rich $z = 0.18$ cluster A1689, we found a steeper than isothermal profile beyond 300 h^{-1} kpc radius.[25] Some clusters at high redshift are nearly as compact in mass. In rich compact clusters mass appears to trace the cluster red light, on scales of a few $\times 100\ h^{-1}$ kpc, with rest-frame V band mass-to-light ratios of a few hundred h in solar units. Weak lens tomographic studies of the outskirts of clusters with the Big Throughput Camera (see below) show that mass density falls rapidly at large radius as expected in models of structure formation, but there are often other interesting mass concentrations nearby.

The mass core radius is smaller than most observed X-ray core radii in nearby clusters, suggesting that the X-ray gas may be less relaxed dynamically than the dark matter. Over the past decade, theoretical CDM N-body simulation mass core sizes have evolved steadily downwards, past the observed mass cores, towards a singular distribution. In 1990 we reported a (30-50 kpc) mass core radius much smaller than the X-ray core (and then current N-body simulation cores). By 1998 the N-body simulations have high resolution and give mass cores much smaller than our observed mass cores (still 30-40 kpc). At least for rich clusters these lens studies appear to confirm the large mass which was implied by virial calculations using velocity dispersions.

Because faint blue galaxies become more common at redshifts above 0.5, most studies of weak lensing have been confined to lenses around redshift 0.2 to 0.4. However, clusters exist at higher redshift and two of them near $z = 0.8$ have been studied recently by weak lensing.[26] As multiband deep imaging becomes more common in lensing work, color-redshifts will enable weak lens studies of clusters at higher redshift. Figure 12 shows an example of weak lensing reconstruction of mass, with 1st order strong lensing corrections included. See also Squires *et al.*1997.[27]

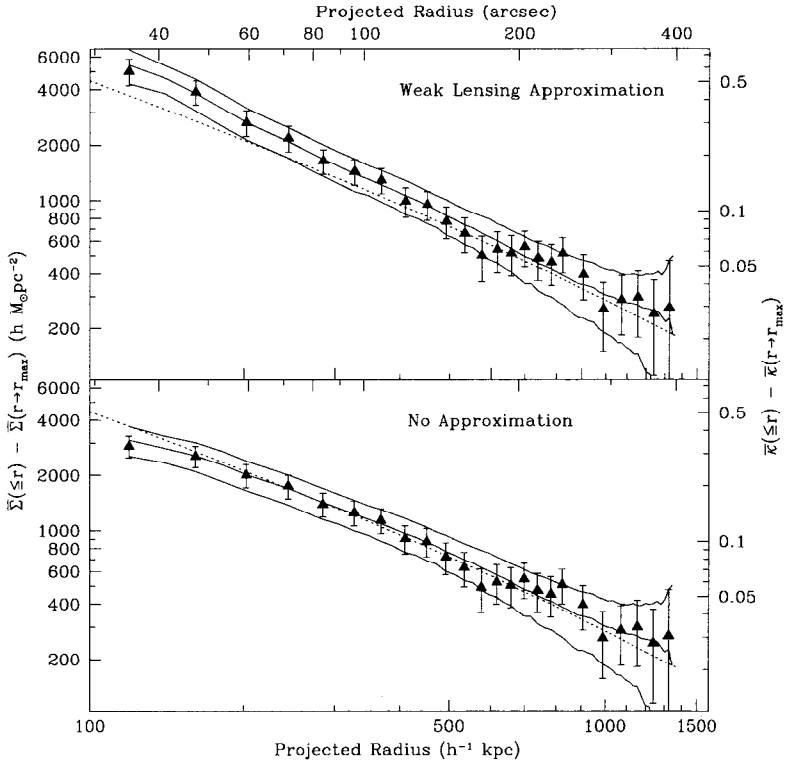

Fig. 12. The radial mass distribution of the cluster RXJ1347, with and without strong lensing corrections,[28] as in Equation 3. The cluster RXJ 1347.5-1145, at a redshift of $z = 0.451$, has an X-ray luminosity $L_X = 2 \times 10^{46}$ erg s^{-1}. $\kappa = \Sigma/\Sigma_{crit}$.

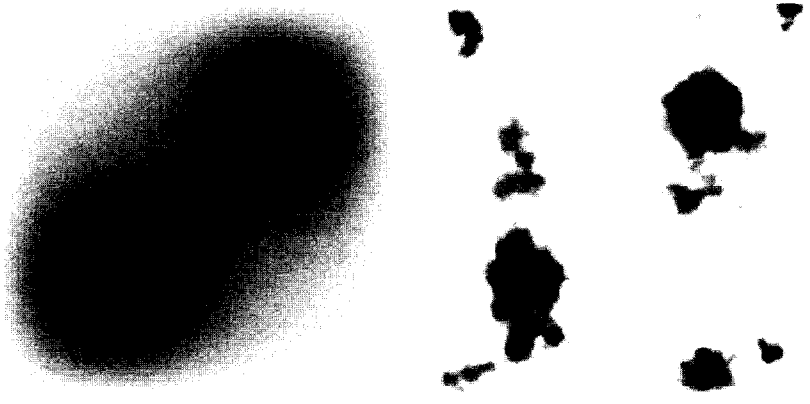

Fig. 13. A test of the low level shear detection. In this simulation, two dwarf mass concentrations [*left*] cause a small shear perturbation in the background galaxies. Weak lens inversion using 11,000 arclets recovers the masses [*right*] at high significance. Shear noise in this simulation is 0.003 and scales as $N_{arclets}^{-1/2}$.

9.1 Detection Limits

Cold dark matter models predict a filamentary structure of mass emerging by redshift 0.5, with peak densities of $10^5 \rho_c$. But most of this dark matter is distributed in less spectacular mass concentrations, with projected (two-dimensional) densities less than $\Sigma_c \sim 1$ g cm^{-2} and rms fluctuations around 0.02 Σ_c. What are the chances of detecting these low level mascons with gravitational lens tomographic searches?

Simulated low level shear in a CCD survey for dark matter is shown in Figure 13, where two dwarf cluster masses (ten times smaller than those discussed above) were placed at redshift 0.3 in a three-dimensional distribution of galaxies extending out to redshift 3. These mascons had 40 arcsec wide soft cores, 600 km sec^{-1} velocity dispersion, and an outer mass cutoff at 500 arcsec. This corresponds to a projected density of $0.06\Sigma_c$.

This simulates a small 2000 times 2000 pixel part of the field of the Big Throughput Camera, in moderate seeing (0.9 arcsec FWHM) and including all blue galaxies to 26th magnitude. This is representative of most of the data we already have, so we wanted to see how far we could push the mass detection. In this inversion we also wanted to push the angular resolution, so we used an inner radius (Gaussian filter) of two arcminutes. Random noise in the inversion is about 0.003 Σ_c and the peak densities in the reconstructed mass map are 0.014 Σ_c. In other words, due to depolarization due to seeing and ellipticity scatter and noise, our efficiency of mass reconstruction was $0.014/0.06 = 0.23$ and the resulting signal to noise ratio for recovery of the two mascons was 5. Dividing by the shear-to-mass efficiency, the rms mass noise is recalibrated to $0.013\Sigma_c$, smaller than the rms in CDM theories. No false mascons with the density of these two test masses were found in the reconstructed mass density image or in repeated realizations. The input diffuse mascons were thus detected at high significance. Larger smoothing filters in the inversion produce somewhat lower shear-to-mass efficiency but much lower false mascon rates and higher significance for overdensities covering large angles.

What will ultimately limit tomographic mass detection? There are two sources of noise and one source of systematic error. The photon shot noise from the night sky diffuse surface brightness may be overcome with longer integration times. In the same way, higher redshift (fainter) galaxies may be reliably photometered. This raises the efficiency, especially for higher redshift lenses. But the source galaxy random ellipticity orientation noise will remain about $e_{rms} = 0.3$, so lower level mass density detections will have to use lower angular resolution, capitalizing on the root N averaging of source ellipticity noise over larger resolution elements. There is also a more fundamental limit due to systematic shear error due to the finite number density of point-spread-function calibration stars. Rms shear variation of stellar images has been reduced to levels of 0.0007 averaged over a 45-arcminute field. Most of this is systematic and fixed, and is due to the optics. This may be calibrated to better than 0.001 per square arcminute, but there remain induced systematics from focus variations. This ultimately limits one arcminute resolution mass reconstructions to about 0.002 Σ_c, even in multi-color deep imaging to 27th magnitude. This is over ten times lower than the rms mass density fluctuations in blank fields predicted in any CDM model. Lower limits may be reached by varying the camera rotation angle.

10 Large Scale Dark Matter

By concentrating on the largest luminous structures known, clusters of galaxies, we are biased to radiation. We have in effect been looking under the lamp post for dark matter. Does light trace mass under all conditions? Larger scale applications of this dark matter mapping may eventually find clumped dark matter unrelated to galaxies or clusters of galaxies. Mosaics of CCDs make such a large scale search for coherent alignment in the distant faint galaxies particularly attractive, and dark matter on angular scales up to degrees can in principle be studied in this way. Dark matter may exist in places where there is no current star formation activity. Larger scale applications of this dark matter mapping may eventually find clumped dark matter unrelated to galaxies or clusters of galaxies; I will show a deep image of a good candidate.

If we wish to extract only information on the statistics of the foreground mass overdensities, rather than map them, there is a tensor statistic analogous to the scalar two-point correlation function.[29,30,23,31,32] All pairs of galaxies separated by some angle on the sky are summed separately in bins of mutual orientation. This integral tensor statistic called the orientation correlation function (OCF) is then built from these summed orientation data. The OCF has both parallel and orthogonal orientation components, each a function of angle on the sky. The OCF detects an excess over random for background galaxies to be oriented parallel or orthogonal to one another. In this way much larger areas of the sky may be covered and a smaller amplitude statistical mass fluctuation spectrum may be detected.

The observational challenge in low shear measurement is systematic errors due to variations across the detector of the point spread function, optics astigmatism, and variable field distortion due to atmospheric refraction. These systematics can be overcome by chopping and trailing techniques, and optics calibration in rich star fields. Preliminary measurements of the arclet orientation correlation function in random fields yield shear correlations which are below the SCDM prediction. The key in finding the rest of the dark matter, even in places where there are no clusters, is to measure shear over much larger areas. This also means that systematics will have to be controlled at the 0.1-0.5 percent shear level. With Gary Bernstein at U. Michigan, we have built a large area blue-sensitive CCD mosaic camera for the four-meter Blanco telescope at CTIO. With this instrument we have a chance of viewing mass in ordinary places, rather than in the inner parts of massive rare overdensities.

11 Large CCD Mosaic

The Big Throughput Camera is so named because it was the only operating large mosaic of back-illuminated CCDs, giving it much more throughput than other mosaics with comparable field of view, as well as good blue sensitivity.[33] [Note: the Sloan CCD mosaic just had its "first light"; this is a much bigger array of the same type of CCDs as the BTC.] The format is a 2×2 array of thinned, broadband antireflection-coated 2048×2048 SITe CCDs. The four-CCD mosaic in the BTC covers an 11.7×11.7 cm area. Mounted at the prime focus of the four-meter Blanco Telescope at CTIO, the 24 micron pixels subtend 0.43 arcseconds on the sky, providing a 34.8 arcmin field of view. Each CCD is separately adjustable in position to $\sim 5\,\mu m$ accuracy and cooled to 170 K.

The BTC's large field of view is ideal for searches for rare objects or events, statistical studies of large numbers of objects, and studies of anything which covers large angular scales. In its year of operation the BTC has been used by a group searching for faint quasars and two groups searching for high-redshift supernovae (20 discovered per night!), which can be used to constrain fundamental cosmological parameters. For the first time, large numbers of high-redshift supernovae are being discovered: 32 identified in first-year BTC images have been confirmed and announced by one team, and a similar number has been found by the other team. A search for Kuiper belt objects is being conducted.

Our studies of large-scale dark matter distribution using weak gravitational lensing exemplify the other two typical uses of the BTC, amassing large-number statistics and covering large angular scales. In weak lensing, the signature of intervening concentrations of dark matter is a small nonrandom component induced in the otherwise random orientations of background galaxies, hence large-number statistics are required. In addition, large angular fields are required to trace the full extent of the dark matter.

We require a large contiguous field of view. The gaps are filled in with "shift-and-stare" exposures, with large shifts of about 1000 pixels (7 arcmin). After about 18 exposures, a contiguous field of 47 arcminutes is covered. The unique problem of large focal-plane mosaics is field distortion, since they cover most of

the usable field of view of large telescopes. In the case of the BTC at the Blanco telescope, the prime focus corrector induces a radial distortion of about 60 pixels, or a few percent, at the corners of array. In addition, the corrector lenses over each of the CCDs introduce a small additional distortion, differential refraction over 35 arcmin is significant and constantly changing in direction, atmospheric pressure variations can cause changes in the focal plane scale from exposure to exposure, and the small field rotation caused by the slight polar misalignment of the telescope is evident over this wide a field. Without correction for these effects, multiple shifted exposures cannot be combined into a single deeper image.

These effects are corrected using a parametric model of the entire optical system and observations of astrometric standard fields from the United States Naval Observatory at a variety of airmasses with each filter used in the observing run. The observed star positions provide constraints on our model of the optical system in which parameters such as the amplitude of the radial distortion and its center relative to the BTC center are allowed to vary. The fit generally converges to a solution with an rms scatter of 0.3 pixels, or 0.13 arcseconds. We then apply the model with its best-fit parameters to our science observations, and for some applications such as surveys, tenth-arcsecond accuracy is more than sufficient. However, higher accuracy is required for our gravitational lensing studies. This is because gravitational lensing analyses are based on image shapes, and shapes on a combined frame can be significantly altered if the image positions differ by even a tenth of an arcsecond on the individual frames. Therefore, for each set of images to be combined, we derive an additional third-order polynomial distortion to each exposure by forcing the coordinates of high signal-to-noise objects to agree among exposures. The residuals from this fit are about 0.06 pixels, or 26 milliarcseconds.

In gravitational weak lens shear measurements one must be particularly careful that the point-spread function (PSF) is not systematically out of round. We have found that astigmatism in the telescope optics is the dominant cause of stellar profile ellipticity systematics. We convolve the image with a flux-conserving kernel designed to circularize stellar images. Astigmatism combined with phase diversity across the chips means that the ellipticity and position angle vary with position, so we construct a position-dependent kernel by fitting a fourth-order polynomial function of x and y to the observed moments of those objects which appear to be stellar. The convolution step adds a minimal amount to the stellar image size, on the order of a few percent, while reducing stellar ellipticities by a factor of ten or more, to less than 0.001. The flow diagram for this pipeline software is shown in Figure 14.

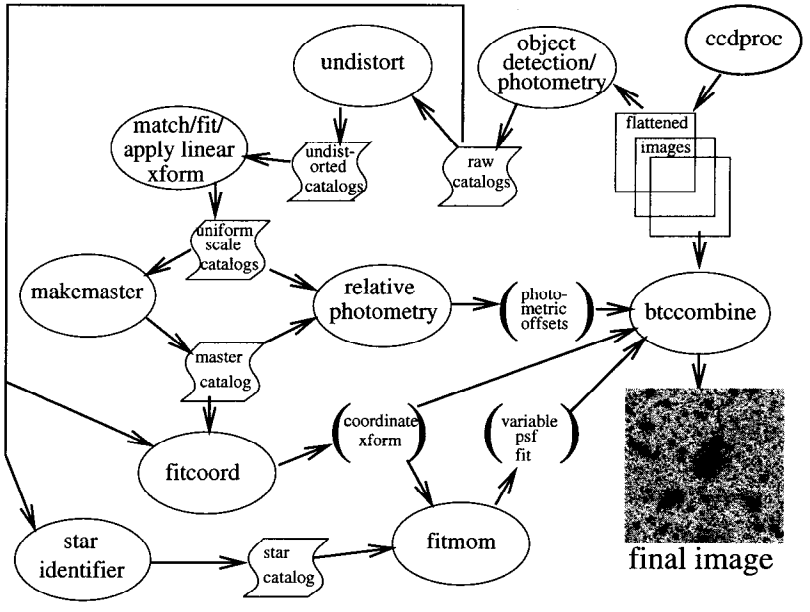

Fig. 14. The data flow in the Big Throughput Camera data reduction pipeline. The observed shapes of stars in the field are used to correct for low-level residual astigmatism.

11.1 Prospecting for Dark Matter

Different CDM cosmologies naturally give rise to differing mass clustering over time. For example, ΛCDM in a flat universe (consistent with current CMB observations) produces an older, larger universe today. These contrasting scenarios can now be tested.

Until recently there have been no tools which could map mass directly on 0.1 - 10 Mpc scales, without reference to luminosity, in an unbiased way. Gravitational lens inversion is now a mature field, and has yielded mass maps over a variety of mass and length scales, from 5 kpc to 2 Mpc. So far, lens search programs

have concentrated on obvious clusters of galaxies where one knows there is a deep gravitational potential well coincident with the luminous baryons. But this is "searching under the lamp post"; in so doing we build in a bias between mass and luminosity. Weak lensing analysis can now be applied to blank fields to explore mass generally, without resort to light. Furthermore, evidence is mounting from strong lensing observations that the input physics for the N-body work is incomplete. It is fair to say that the process of mass clustering is not yet well understood.

The recent primordial deuterium measurement together with the observed high cluster baryon density (the "baryon catastrophe"), indicate $\Omega_{\rm matter} = 0.4$; this is also predicted by large-scale peculiar velocities. This additional mass in dark structures, over what has been inferred from studies of clusters, will be clustered throughout a deep probe out to high redshift. The clustered mass lenses the high redshift galaxies and is visible in gravitational lens tomographic maps. Such a mass probe of random areas relies heavily on wide-field deep imaging in superb conditions and over a wide wavelength range. While deep lensing probes of many blank fields will be necessary in order to test this and measure the cosmic variance, a hint of what may be in store is shown in Figure 15. A large mass structure with peak mass density of $0.02\Sigma_c$ is found in a BTC field chosen for its absence of obvious clusters of galaxies. In some blank fields examined in this way with the BTC, we have found high redshift clusters by first detecting the mass overdensity via weak lens inversion. In a BTC survey of "normal clusters" chosen by their below average X-ray luminosity, multiple mass concentrations with occasional mass bridges connecting them are found.

12 Cosmic Complementarity

The observational situation in the $\Lambda - \Omega_M$ plane, mid-1998, is reviewed in Figure 16. Three complementary experiments are plotted. Recently, two groups (the Supernova Cosmology Project and the High-z Supernova Team) using Type Ia supernovae as standard candles (objects of known luminosity) and assuming that their flux measurements were not contaminated by sample selection, evolution, or dust systematics, both conclude that the expansion of the Universe is accelerating rather than decelerating (i.e., $q_0 < 0$). If correct, this implies that much of the energy in the Universe is in an unknown component. The simplest explanation is

Fig. 15. The mass density reconstructed from 8700 blue arclets in moderately deep BTC integrations in a field devoid of known clusters. A large low-level (shear 0.02) mass is discovered. Note other mass concentrations in this clusterless "blank" field. Keck spectroscopy has just been obtained for 28 galaxies in the mass concentration shown in this field.

a cosmological constant with $\Omega_\Lambda \sim 2/3$. My estimate of the likelihood contours are shown.

The pattern of anisotropy in the CMB depends upon the total energy density in the Universe. The first acoustic peak in the multipole power spectrum is $l_{\rm peak} \simeq 200/\sqrt{\Omega_M + \Omega_\Lambda}$. These current likelihood contours are shown as dashes. The CMB anisotropy does not measure mass at $z = 1000$ directly; a model relating three mass-derived effects on the radiation must be fit to the CMB anisotropy data. Note that the likelihood contours for these first two experiments are roughly orthogonal; as the new generation of satellite CMB observations map out the fine scale structure of the microwave sky, the position our Universe occupies in this plane will be strongly constrained.

Finally, as direct lensing observations of dark matter explore more of the Universe, the vertical bar marked "known matter" will move to the right. The black-grey shading going up to higher Ω_m denotes the situation if future explorations for dark matter discover significant high M/L structures in the vast regions between clusters. It will be interesting, and a test of our cosmological model, if the results of all three tests (SN, CMB, and Lensing) are consistent. It will be even more interesting if they are not. Such a dark matter and dark energy survey is feasible, using current technology.

13 Dark Matter Telescope

One might ask why we need any new facilities in astronomy, given the fantastic advances made possible with the Hubble Space Telescope, the Keck Telescopes, and the imminent Gemini telescopes. The Hubble Space Telescope is a relatively small (2.4 meter) and expensive telescope offering the finest possible resolution, making it ideal for studies of stars and tenth-arcsecond features in galaxies. The Keck Telescopes offer unparalleled collecting area, focused on small-area imaging and spectroscopy of the faintest and most distant objects. The Gemini telescopes will combine superb light gathering power with IR capability. All of these telescopes, however, have relatively small fields of view and are operated in the traditional mode for astronomy: a given project is pursued for at most a few nights at a time, after which a different group of astronomers uses a different instrument to pursue a different scientific goal. This mode of operation is necessary for projects which serve large communities with varied scientific interests, but it requires compro-

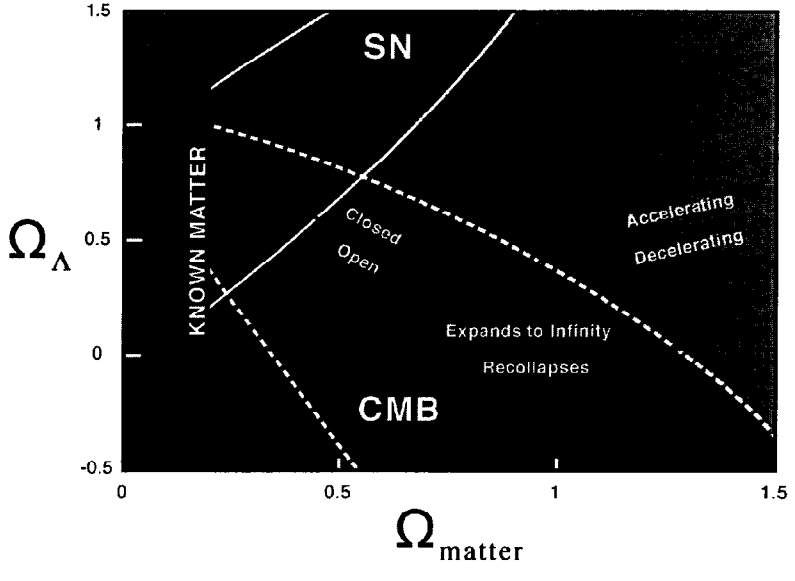

Fig. 16. The current situation in the cosmological constant-matter plane. Three key experiments are indicated: Supernova measurements of the acceleration (SN), cosmic microwave background anisotropy measurements (CMB), and direct measurements of mass (shading). All three will see vastly decreased errors in the next few years. The "known matter" is a lower limit based on extrapolating cluster masses to the field, assuming identical M/L ratios. As more mass is found, this vertical black bar will move to the right. Note that the recent determination of the cosmic abundance of deuterium suggests $\Omega_{matter} = 0.4$.

mises in the design of the telescope, and precludes the pursuit of projects which require very large amounts of data and telescope time.

Several recent projects present a different model for the pursuit of astronomical science goals, whereby a telescope is completely dedicated to one or two important projects for a period of years. An example is the Sloan Digital Sky Survey, for which a dedicated 2.5-meter telescope and instrumentation have been built. This project will yield a high-quality digital map of the entire northern sky, plus redshifts of several million galaxies and quasars.

A definitive measure of the density spectrum of the dark matter on supercluster scales is technically within reach. Deep imaging of millions of distant galaxies at several wavelengths (to get statistical redshifts from their colors) repeated in many different directions would have the precision to detect a fraction (less than ten percent) of the statistical weak lensing shear predicted by current Cold Dark Matter theory. An accurate measurement in 25-degree areas of the sky, to get the cosmic variance, would provide a direct measure of mass content and the mass fluctuation spectral index. With a dedicated six-meter "Dark Matter Telescope," an advanced mosaic of CCDs covering over a degree, and deep imaging in multiple wavelength bands, this project would take five to ten years to complete. The payoff in our understanding of dark matter and cosmology would be well worth the effort.

We propose, therefore, the construction of a six-meter class telescope with a single instrument optimized for the pursuit of a single goal: measurement of the distribution of dark matter in the Universe. The massive clusters, however, are like the whitecaps on the ocean. To really answer the central question in cosmology, "where is all the mass in the Universe?", we must study the "ocean" directly. The proposed Dark Matter Telescope will do this, showing where the dark matter is, how it clumps, and thus limiting the possible candidates for its constitution. If the fields are chosen appropriately, these same data may be used to map the inner part of the Kuiper belt of comets, and high-redshift supernovae, discovering thousands of these objects in a few years. Indeed, the supernova database will be an important constraint on cosmology and dark matter. So the dark matter mapping and supernova survey would use the same imaging data and yield related cosmological data on both the dark energy and mass budget of our universe.

The distant star-forming galaxies form half of the toolbox required for this unique cosmological probe. The rest of the tools are a wide-field CCD mosaic and a special wide-field low-aberration optical telescope with state-of-the-art light gathering capability and 350-900 nm wavelength coverage. To undertake this tomographic gravitational lens reconstruction of dark matter images at high redshift and large look-back times requires superb imaging of distant background galaxies. At 29th magnitude, there is a distant blue galaxy every arcsecond on the sky. Because the surface brightness of these distant galaxies falls as the 4th power of the redshift, these distant galaxies are so faint that existing telescopes with their relatively small fields of view would spend weeks of telescope time to produce only a narrow pencil beam probe. One requires superb angular resolution over a two to three degree field, coupled with the light gathering power of a large six to eight meter mirror. The Dark Matter Telescope would require superb blue-red optics and a state-of-the-art wide-field CCD array camera with a total photon throughput well in excess of even the Keck telescopes. Innovative software will be required to handle the flood of data. Unfortunately, present-day telescopes suffer especially from small fields of view, but also from poor image quality and over-commitment, allowing only tantalizing forays into dark-matter mapping. The wide spectral coverage, together with low aberration requirements, are a challenge for normal telescopes which have multi-element glass correctors. A design being seriously discussed is the Paul-Baker three-mirror telescope. This corrects for aberrations and is intrinsically achromatic and non-dispersive. A new-technology Dark Matter Telescope of six-meter aperture would cost approximately 30M 1998 dollars, and the camera would cost an additional 8-15M 1998 dollars. Operations over the period of this survey (ten years) would cost considerably less than ten percent of the capital cost per year because of no instrument changes and no visitor support. The data would be uniformly acquired by a small crew and released to the community.

The Dark Matter Telescope would be much more cost effective and optically efficient than other telescopes because it would be optimized for wide-field surveys. In terms of "throughput" (collecting area times imaging area on the sky), it would be 200 times more efficient than any of the wide-field mosaics now being built for existing or new telescopes, and tens of thousands times the throughput of the Hubble Space Telescope. A special wide-field low-aberration optical telescope in the six-meter class is required in order to take the next step in our understanding of the origin of structure, the dark energy, and mass in our Universe.

Acknowledgments

My principal collaborators in this research are Gary Bernstein, Ian Dell'Antonio, Phil Fischer, Raja Guhathakurta, Ayana Holloway, Greg Kochanski, and Dave Wittman.

References

[1] White, S. D. M., Frenk, C., & Davis, M., 1983, Astrophys. J. 274, L1.

[2] Blumenthal, G., Faber, S., Primack, J. & Rees, M., 1984, Nature 311, 517.

[3] Burles, S. & Tytler, D., 1998, Astrophys. J. 499, 699; astro-ph/9712265.

[4] Zwicky, F., 1933, Helv. Phys. Acta 6, 124.

[5] Zwicky, F., 1937, Phys. Rev. 51, 290.

[6] Dyer, C. C. & Roeder, R. C., 1973, Astrophys. J. 180, L31.

[7] Press, W. & Gunn, J. E., 1973, Astrophys. J. , 185, 397.

[8] Walsh, D., Carswell, R. F., and Weymann, R. J., 1979, Nature 279, 381.

[9] Peebles, P. J. E., 1993, *Principles of Physical Cosmology* (Princeton University Press).

[10] Carlberg, R. G., Lee, H. K. C., Ellington, E., Abraham, R., Gravel, P., Morris, S., & Pritchet, C. J., 1996, Astrophys. J. 462, 32.

[11] Garnavich, P. *et al.*, 1998, Astrophys. J. 493, 53.

[12] Narayan, R, & Bartelmann, M., 1996, astro-ph/9606001.

[13] Evrard, A. E., *et al.*, 1996, Astrophys. J. 469, 474.

[14] Tyson, J. A., Valdes, F., Jarvis, J. F., & Mills, A. P., 1984, Astrophys. J. Lett. 281, 59.

[15] Tyson, J. A., Valdes, F., & Wenk, R. A., 1990, Astrophys. J. Lett., 349, L1.

[16] Im, M., Casertano, S., Griffiths, R. E., Ratnatunga, K. U. & Tyson, J. A., 1995, Astrophys. J. 441, 494.

[17] Blandford, R. D. & Narayan, R., 1992, Ann. Rev. Astron. Astrophys, 311.

[18] Turner, E. L., Ostriker, J. P., & Gott, J. R., 1984, Astrophys. J. 284, 1.

[19] Tyson, J. A., Kochanski, G., & Dell'Antonio, I. P., 1998, Astrophys. J. Lett. 498, 107.

[20] Colley, W. N., Tyson, J. A., and Turner, E. L., 1996, Astrophys. J. Lett. 461, 83.

[21] Schneider, P., Ehlers, J., & Falco, E. E., 1993, *Gravitational Lenses*, (Springer, NY), 244.

[22] Syer, D. & White, S. D. M. 1998, Mon. Nat. Royal Astron. Soc. 293, 337.

[23] Miralda-Escudé, J., 1991, Astrophys. J. 370, 1.

[24] Kaiser, N. & Squires, G., 1993, Astrophys. J. Lett. 404, 441.

[25] Tyson, J. A. & Fischer, P., 1995, Astrophys. J. Lett. 446, 55.

[26] Clowe, D., Kaiser, N., Luppino, G., Henry, J. P., & Gioia, I. M., 1998, Astrophys. J. 497, 61.

[27] Squires, G. *et al.*, 1997, Astrophys. J. 482, 648.

[28] Fischer, P., & Tyson, J. A., 1997, AJ, 114,14.

[29] Gunn, J. E., 1967, Astrophys. J. 147, 61.

[30] Valdes, F., Tyson, J. A. & Jarvis, J. F., 1983, Astrophys. J. 271, 431.

[31] Blandford, R. D., Saust, A. B., Brainerd, T., & Villumsen, J. V., 1991, Mon. Not. Royal Astron. Soc. 251, 600.

[32] Seljak, U. & Zaldarriaga, M., 1998, astro-ph/9811123.

[33] Wittman, D., Tyson, J. A., Dell'Antonio, I. P., Bernstein, G., Smith, D., Lee, R. W., & Blouke, M. M., 1998, SPIE, 3355, 626.